Mass Transfer across Mobile Interfaces

J. B. ANGELO

Esso Research and Engineering, Baytown, Texas

and

E. N. LIGHTFOOT

University of Wisconsin, Madison, Wisconsin

The dependence of extraction efficiency on flow distributions and droplet boundary-layer behavior was investigated in a specially designed sieve-tray extractor. Flow patterns and drop trajectories were obtained from residence-time distributions and photographic observation. Extraction efficiency and continuous phase residence times were determined by a pulse technique.

For most runs, flow behavior could be adequately described by the assumptions of perfect mixing in the continuous phase and plug flow of the drop phase. However, drop velocities were higher than predicted by single drop correlations, and the flow pattern was sensitive to minor changes in operating conditions. Observed extraction efficiencies were in good agreement with predictions based on observed flow patterns and the two film, surface stretch, mass transfer model of Angelo and Lightfoot. Approximately 90% of the stage mass transfer effectiveness appears to be due to the drop rise period, and essentially all the remainder to drop formation for the stage geometry selected.

The greatest obstacle to reliable prediction of extractor performance is uncertainty as to the effect of operating conditions on flow distribution.

While much important work has been done in the field of liquid-liquid extraction, progress in relating equipment performance to fundamental mechanisms has been slow. Prior research in this field has been primarily concerned either with measurement of over-all stage efficiency in scaled down apparatus, geometrically similar to commercial equipment, or with laboratory experiments with drops under somewhat artificial conditions. These research efforts have been reviewed by Olney and Miller (*16*) and by Treybal (*21, 22*).

Determinations of stage efficiency have normally been made in rather small columns, not over 6 in. in diameter in most instances, and have not in general been accompanied by detailed observations of flow patterns or mass transfer behavior within any one stage. Rather, observed stage efficiencies have been correlated with stream rates and physical properties of the test solutions in an essentially empirical manner. While useful, this type of observation is of limited value as a basis for improving column design, or even for scale-up purposes. Additional information has been obtained from residence-time distribution studies (*11, 13*), but these results are still fragmentary.

Stage efficiencies of extraction equipment are often much lower than for other mass transfer apparatus, for example, distillation columns. Of the various types of equipment, the sieve-plate extractor is a particularly appealing device for study because of its simple geometry, high throughput capacity, and desirability as a commercial

TABLE 1. STAGE EFFICIENCIES OF SIEVE-TRAY EXTRACTORS: PERFORMANCE DATA FOR REPRESENTATIVE SYSTEMS OF HIGH INTERFACIAL TENSION

Dispersed phase	Continuous phase	Extracted solute	Tower diameter in.	No. plates	Plate spacing in.	Hole diameter in.	Superficial velocity* ft./hr. Dispersed phase	Superficial velocity* ft./hr. Continuous phase	Over-all plate Eff. %	Reference
kerosene	water	benzoic acid	3.63	11	4.75	3/16	34-162	25-136	5-10	*1*
toluene	water	benzoic acid	3.63	11	4.75	3/16	39-144	36-78	5-10	*1*
toluene	water	diethylamine	4.18	8	6	1/8	26-131	11-78	5-17	*6*
water	toluene	diethylamine	4.18	8	6	1/8	15-150	2	2-15	*7*
toluene	water	benzoic acid	2.72	1	12	0.046	6-9	12	13-30	*8*
toluene	water	benzoic acid	2	6	24	1/8	11-235	92-184	3-16	*14*
water	toluene	benzoic acid	2	6	24	1/8	57-184	4-11	16-38	*14*
toluene	water	benzoic acid	3.06	8	6	1/8	8-70	23-67	2-7	*15*
toluene	water	benzoic acid	8.75	10	6	1/8	12-48	11-37	3-10	*18*
				10	6	3/32	12-48	11-37	3-10	*18*
toluene	water	benzoic acid	3.56	17	3	3/16	10-80	15-31	3-6	*23*
				9	6	3/16	30-77	23-41	5-9	*23*
				6	9	3/16	36-79	23-39	7-13	*23*

* Based on column cross section.

device. In small laboratory columns with partially miscible systems ($\sigma < 10$ dynes/cm.), over-all stage efficiencies as high as 80% have been observed (*14*). However, in most cases, over-all efficiencies of from 5 to 40% were observed with the bulk of the data below 20% (*1, 6* to *8, 14, 18, 21*). Performance of most industrial extractors is not much better. Typical experimental efficiencies for systems of high interfacial tension ($\sigma > 20$ dynes/cm.) are given in Table 1.

Mechanically agitated extractors, such as pulsed sieve-plate columns do give higher efficiencies (*16*), and it is believed that such application of additional energy is necessary to provide adequate dispersion for systems of higher interfacial tension. Practical application, however, appears limited to situations where relatively high power requirements are not of critical importance.

Therefore, it is important to determine in detail the factors responsible for the low efficiency of the simpler gravity flow devices, such as sieve-plate extractors, to assess the possibility for improving their performance. In spite of the many investigations made on this type of equipment (*16, 21, 22*), no detailed explanation for the observed low efficiencies is readily available.

It is the purpose of this work to supply such an explanation for at least one representative type of equipment, a sieve-plate column, under realistic operating conditions, and to indicate the areas of fundamental importance most needed for further investigation.

EQUIPMENT AND PROCEDURE

Materials

The *continuous* phase used in all runs was distilled water and the drop phase was a highly paraffinic petroleum fraction, known as *Isopar-H*, with a boiling range of 350-375°F. The water was prepared in a stainless steel Barnstead still equipped with a de-ionizer and a charcoal sorber. The Isopar was specially distilled by the Baytown refinery of the Humble Oil and Refining Co. It has a specific gravity of 0.757, a viscosity of 1.30 centipoises and an interfacial tension of 48.5 dynes/cm. at 74°F.

The tracer used to determine residence-time distributions was the Isopar-insoluble dye Amaranth Red number 2 FD and C, which exhibited maximum light absorption at 520 mμ. Up to the maximum concentration used in this study (0.03 g./liter), the dye followed Beer's Law and had no detectable effect on surface tesnion.

The solutes used to measure mass transfer effectiveness are presented in Table 2. These also followed Beer's Law and had no apparent effect on surface tension. Because of their high optical absorptivity these solutes permitted measurement of mass transfer effectiveness without appreciably affecting system physical properties. The independence of their distribution coefficients of concentration permitted use of a pulse technique for determining the stage efficiency.

Equipment Geometry

The model extractor used in this research is shown schematically in Figure 1. It was fully equipped with piping, pumps, rotameters, and solvent storage facilities, and was well instrumented. The major item of instrumentation was a Beckman D B Spectrophotometer, fitted with a flow cell and connected to a recorder for continuous monitoring of absorbance of percent transmittance.

This extractor was designed to facilitate detailed observation and measurement of fluid mechanic and mass transfer behavior, and yet be reasonably representative of industrial size equipment. To achieve these objectives a rectangular construction was chosen. It permitted use of large tray height and width at relatively small solvent flow rates and, at the same time, direct photographic observation of both the dispersed and continuous phases.

The experimental extractor was made of nickel plated brass and plate glass, and all wetted surfaces were of glass, nickel, no. 316 stainless steel, Teflon, viton, or (for water storage only) polyethylene. No greases or other possible surface contaminants were used; pipe threads were lubricated with

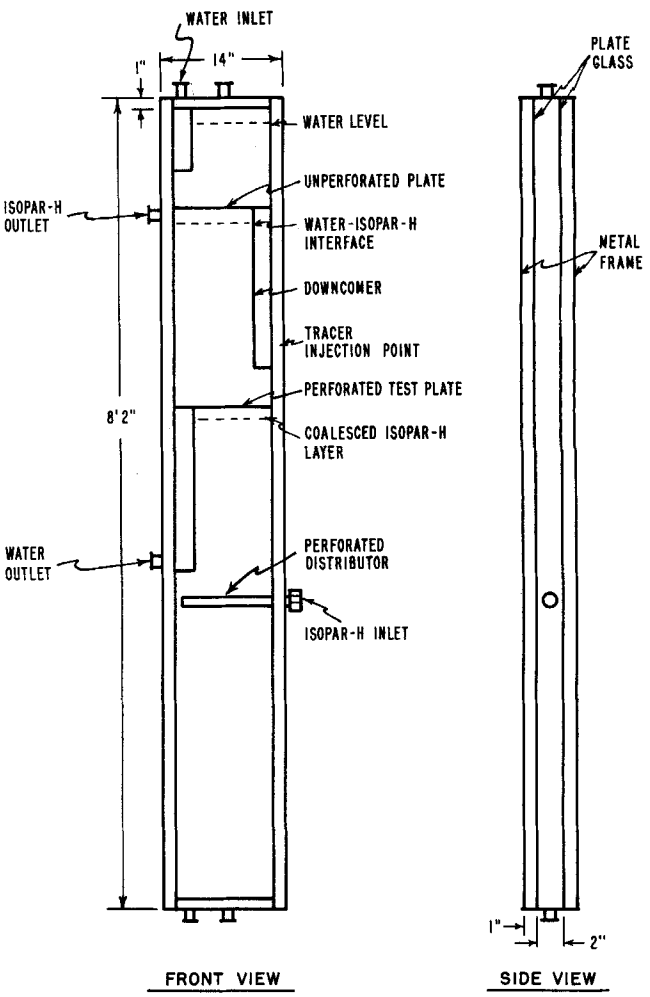

Fig. 1. Schematic diagram of the model liquid-liquid extractor.

TABLE 2. CHARACTERISTICS OF SOLUTES USED FOR EXTRACTION AND TRACER STUDIES AT 74°F

Solute	Distribution coefficient $m = \rho_{AI}^*/\rho_{AW}^*$	Maximum concentration g./liter Water phase	Maximum concentration g./liter Isopar-H phase	Optical Properties: Extinction coefficient e†, sq.cm/g. Water	Extinction coefficient e†, sq.cm/g. Isopar-H	Wavelength used mμ Water	Wavelength used mμ Isopar-H
1. benzyl alcohol	0.182	1.00	0.20	1.804×10^3	1.644×10^3	257	259
2. dl-α-methylbenzyl alcohol	0.590	0.50	0.30	1.766×10^3	1.443×10^3	257	258
3. acetophenone	10.268	0.01	0.10	98.46×10^3	7.473×10^3	245	279
4. Amaranth no. 2 FD and C dye	—	0.03	—	38.38×10^3	—	520	—

† Defined by absorbance $A = \ln (I_0/I_x) = \rho_L x/e$ where I_0 is incident light intensity, I_x intensity transmitted through a layer of solution at concentration ρ_L and thickness x.

Teflon tape, and O-rings sealing the extractor were of viton. These materials greatly simplify the problem of avoiding surfactant contamination.

The horizontal cross section of the extractor was rectangular with a width in the direction of crossflow of 12 in. and a thickness of 2 in. The test tray contained fifty-eight ⅛ in. punched plate orifices (*14, 21*) on a ½ in. triangular pitch. Orifice design, hole diameter, and tray spacing corresponded to recommended (*21*) designs.

Teflon gaskets were used to form a tight seal between the metal trays and the plate glass faces, and the column was designed to disperse the light liquid.

In addition, this column contained some special features such as additional large exit and entry ports to permit segregation of the continuous phase from one tray without affecting the over-all flow patterns in the column. Furthermore, the topmost tray was left unperforated to permit continuous withdrawal of the dispersed phase immediately after it passed through the test stage. Side entry ports were provided to permit the addition of dye streams, or other tracers in either phase.

Procedure

Operation of the extractor was carefully standardized, and the same procedure was used in all runs, regardless of the measurements being made. In addition, each run was preceded by a thorough pretreatment designed to remove surfactants and small dirt particles which might affect interfacial behavior. Experiments were conducted at from 72° to 78°F. and atmospheric pressure.

Cleanliness is an important feature in liquid extraction systems since surfactants such as oils, greases, decomposition products of rubber gaskets, solvents, and hydrated metal oxides can easily result in reduced extraction efficiencies. Therefore, prior to experiments, the system was flushed thoroughly with a dilute solution of an acetone-methanol mixture in distilled water. The glass front plate was removed and all inner surfaces washed with the acetone-methanol-distilled water solution, followed by a mild detergent and rinsed many times with warm distilled water. Storage tanks were disassembled and cleaned separately. Everything was reassembled and the column filled with warm distilled water, allowed to sit for a few hours, drained completely, and refilled.

With fresh solutions of both distilled water and Isopar-H placed in their respective reservoirs and the column completely filled with the water (continuous) phase, the system was ready for the extraction operation.

A flow diagram of the system is shown in Figure 2. The water phase entered at the top of the column via a rotameter, passed through the test stage and left through a port near the bottom of the lower downspout. Provisions were made for either discarding this stream (during residence-time and stage efficiency determinations) or recycling it (during saturation of the two phases). During residence-time determinations it was sampled continuously.

With the water phase flow rate at its desired value, the Isopar-H phase was pumped into the system through a second rotameter and dispersed into droplets by a stainless steel distributor. The flow rate of this phase was adjusted to its desired value. The dispersed Isopar-H phase rose to the bottom of the test tray, coalesced into a layer roughly ½ in. in depth, and was redispersed into drops which entered the test stage. Drop formation at the orifice plate was unpredictable because many holes were not working and the pattern of working holes was not stable at the relatively low flowrate used. The drops moved upward through the water phase which entered just under the downspout from the top tray. Rising through the test stage, the Isopar drops formed another coalesced layer under the top tray (unperforated) and left through an adjacent sideport. This stream was either recycled back to its reservoir (residence-time determinations) or collected separately (stage efficiency determinations).

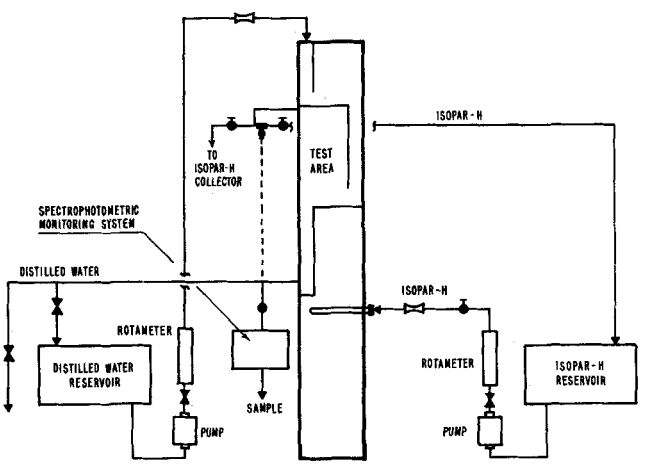

Fig. 2. Simplified flow diagram of extraction system.

To prevent drop of the water level at the top of the column, and the interface level below the unperforated plate, manual control of the flow rates of both leaving phases was maintained. Only slight adjustments were necessary, however, since the column operated quite stably. Throughout each run the liquid level at the top of the column was held constant to assure a constant water flow rate. The interface level beneath the unperforated plate was held about 2 in. below the outlet port during both residence time and stage efficiency runs. This prevented carry-over of water with the Isopar-H leaving the stage.

During operation, the accumulation of interfacial dirt or rag between the two liquid phases, which is common to the operation of such units (*21*) was not ordinarily present; continuous flushing of the interface was thus unnecessary. The exact nature of this interfacial rag is unknown, but it is at least partially due to oxidation. Paraffins such as kerosene or Isopar seem resistant to rag formation; in particular, Isopar is even stable to permanganate oxidation and only slightly affected by fuming sulfuric acid.

Operation of this extractor is such that the water phase only passes through the test section and does not enter the sealed lower half of the extractor containing the Isopar-H distributor. Although this sealed section is full of water, it was not continuously renewed with fresh water during operation.

MEASUREMENT TECHNIQUES

Residence-Time Studies

Residence time probability distributions such as those shown in Figures 6 and 7 were obtained for the continuous phase in the model extractor through use of an effectively instantaneous pulse of tracer material, Amaranth Red Dye. This dye was injected into the water phase as it entered the test stage under the upstream downcomer (see Figure 1), with a hypodermic syringe and in the direction of flow. The dye was injected at a fast steady rate in about five seconds or less. The effluent water stream concentration was sampled and continuously monitored by means of the Beckman D B Spectrophotometer and Recorder, thus generating a curve of absorbance as a function of time at the desired wavelength (520 mμ). In addition, simultaneous motion pictures (32 frames/sec.) were made of the changing dye patterns at the existing flow conditions. These movies provided qualitative observations of the stage to supplement the residence time curves. For typical flow conditions 98% of the injected dye was recovered in 5 to 6 min. of continuous steady operation of the extraction stage after a pulse injection of tracer.

Stage Efficiency Studies

The same pulse injection technique was used to obtain the stage efficiency except that the tracer material (see Table 2) was partially extracted out of the continuous water phase by the Isopar-H droplets. Pulse volumes of 50 to 100 cc. were necessary to produce measurable concentrations in the effluent Isopar stream from the top of the test stage. This was due to limited solute solubility and recorder sensitivity. A pulse technique was especially appealing here since it avoided recovery problems and

shortened runs. This was highly desirable from the standpoint of the Isopar-H since it was difficult to handle and store safely.

Use of the pulse technique is justified by the linearity of the systems studied; total molar concentrations, distribution coefficients, and solute diffusivities could all be considered constant for the experimental conditions used.

Measurements were made in the same way as for the residence time experiments. However, since the fraction extracted by the Isopar phase was low (2 to 10%), the Isopar phase was sampled instead of the water phase, as was done previously in the residence time determinations, the recorder was adjusted to read full scale from 90 to 100% transmittance and transmittance rather than absorbance was recorded. Material balances on the diffusing solutes could not be obtained due to equipment limitations in monitoring the concentration of both the Isopar-H and water phases simultaneously.

Table 3. Drop Distribution for Isopar-*H* Drops in Water for Test Stage in Model Extractor

Less than D_i cm.	Drop fraction* n_i/N	Average Velocity† $(v_{zi})_{avg.}$ cm./sec.	Slip Velocity‡ $(v_{zi})_{slip}$ cm./sec.	Terminal Velocity§ $(v_{zi})_t$ cm./sec.	Residence Time¶ t sec.	Reynolds no.# $D(v_{zi})_{avg.}\rho_C/\mu_C$	Weber no.# $D(v_{zi})^2_{avg.}\rho_C/\sigma$
0.05	0.0000	—	—	—	—	—	—
0.10	0.0036	—	—	—	—	—	—
0.15	0.0228	9.27	6.93	4.79	5.93	121	0.22
0.20	0.0313	9.72	9.90	7.20	5.66	177	0.34
0.25	0.0370	11.79	12.59	9.10	4.66	276	0.64
0.30	0.0550	12.13	14.67	10.45	4.53	347	0.83
0.35	0.0420	13.99	16.35	11.63	3.93	473	1.31
0.40	0.0455	14.69	17.84	12.49	3.74	573	1.67
0.45	0.0512	14.83	18.98	13.06	3.71	655	1.93
0.50	0.0548	15.83	19.89	13.67	3.47	783	2.45
0.55	0.0612	17.19	20.24	14.09	3.20	940	3.20
0.60	0.0747	17.46	20.53	14.37	3.15	1045	3.61
0.65	0.1152	17.11	20.78	14.74	3.21	1114	3.77
0.70	0.1458	17.45	20.99	15.16	3.15	1227	4.24
0.75	0.1287	17.04	21.17	15.20	3.23	1286	4.35
0.80	0.0683	17.36	21.33	15.23	3.17	1401	4.82
0.85	0.0313	17.77	21.23	15.27	3.10	1527	5.37
0.90	0.0235	18.07	21.14	15.29	3.04	1647	5.89
0.95	0.0028	17.17	21.19	15.23	3.20	1654	5.62
1.00	0.0014	—	—	—	—	—	—
1.05	0.0000	—	—	—	—	—	—
1.10	0.0036	—	—	—	—	—	—

* 1,406 observations
† 876 observations
‡ Estimated from the correlation of Liou (24)
§ Estimated from correlation of Hu and Kintner (*10*)
¶ Based on effective stage height of 55 cm. and $(v_{zi})_{avg}$
# Based on average drop size in class interval.

Photographic Studies

A significant part of this research program was the development of photographic techniques to obtain experimental fluid mechanic data for use in predicting stage efficiency. These data included: 1. sizes, velocities, and trajectories of rising drops; 2. droplet interfacial area and volumetric holdup; 3. dispersed-phase residence times; 4. surface area and volume changes, and the presence of internal circulation effects during drop formation; and 5. mixing characteristics of the two phases. Proper lighting of the field of interest was one of the most important problems encountered here. All film was developed under high contrast conditions.

During residence time determinations, low speed motion pictures (32 frames/sec.) were taken to provide additional information for the selection of a realistic flow model. The camera, a Ciné Kodak Special II, was equipped with a Kodak Ciné Ektar lens (15 mm., f/2.5, wide angle). The films were 16 mm. Eastman plus-X Type 7276 Reversal black and white and 16 mm. Kodak Kodachrome II KRA 449 photoflood for color. The entire extraction stage was illuminated by back lighting from four photoflood lamps arranged in a rectangle as illustrated in Figure 3. A piece of translucent tracing paper was used for a diffusing background in which colored drops and dye patterns showed up clearly, but clear drops were not easily visible. This technique was useful for visually following the trajectory of a dyed drop in a swarm and for obtaining its velocity by the double flash technique discussed below.

For making detailed studies of the time variation of surface area and volume for forming drops, high speed photography was necessary since formation times were of the order of 0.10 sec. A Wollensak Fastax motion picture camera was used to photograph forming drops at close range, at 1,000 to 1,600 frames/sec. A 6 in. lens with a 2 in. extension tube was used for observing single drop fields and a 35 mm. lens (with no extension tube) for larger fields containing swarms of drops. The films were Kodak Tri-X negative for high speed.

With such high framing rates, good contrast was highly dependent upon proper lighting. The method developed by Damon, Angelo, and Park (*4*) was used to obtain sharply defined photographs of the Isopar-H drops during formation; a side view of the experimental setup is shown in Figure 4. Drop measurements made from these movies are discussed elsewhere (*2*).

Drop sizes, velocities, interfacial area, and volumes for the rising drops were obtained with a Speed Graphic Camera and two single flash photolights of differing intensity. The Speed Graphic was equipped with Kodak Super XX Panchromatic 4 × 5-in. sheet film and a Wollensak Betax 6½-in. f/2.5 lens. The photographic setup of Figure 5 was used in conjunction with a timing device which

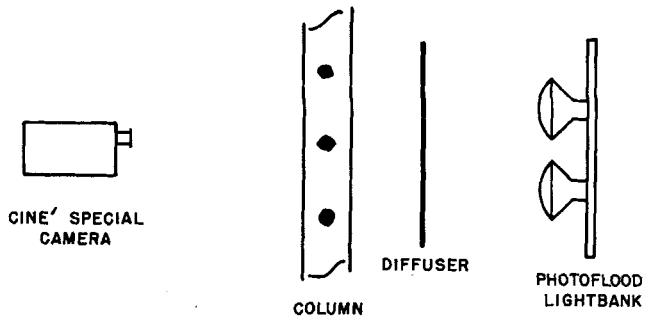

Fig. 3. Photographic setup for illuminating entire stage of drops.

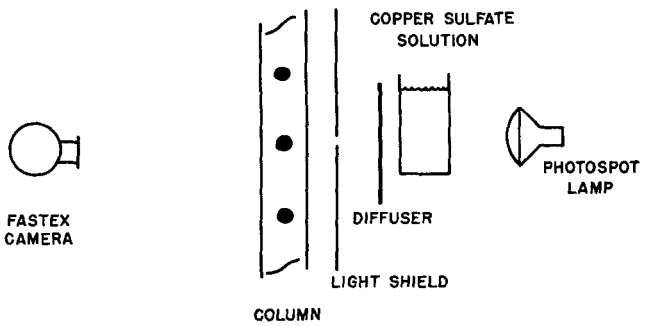

Fig. 4. Photographic setup for detailed observation of drops.

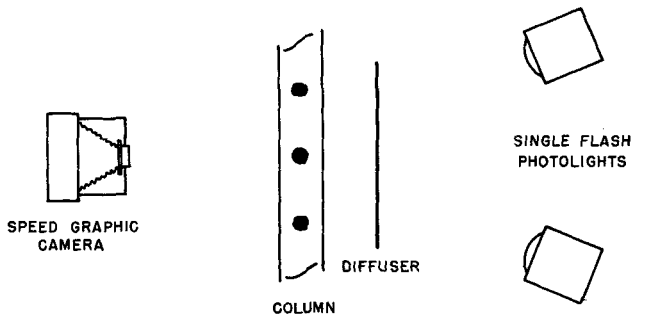

Fig. 5. Photographic setup for double flash exposure of drops.

caused the lights to flash in a preselected time interval (about 0.10 sec.), thereby producing on the negative two images of each drop in the stage. A digital converter was used to measure the drop dimensions and distances between successive drop images, and to punch the data on computer cards for analysis with a digital computer.

The drop velocity was calculated using the vertical distance traveled in the measured time increment. The area and volume of each drop was calculated on the basis that it was either an oblate or prolate ellipsoid, or a sphere. The total interfacial area and volumetric holdup was just the sum of those for each individual drop within the stage (usually about 500 drops).

EXPERIMENTAL RESULTS: FLUID FLOW BEHAVIOR

Continuous Phase

In order to make realistic estimates of the mass transfer behavior of the model extractor it was necessary to establish a flow model for the test stage, upon which to base subsequent calculations. Selection was made on the basis of residence time studies and visual observation of the two phases. Preliminary investigation indicated that for the 24 in. tray spacing used here, conditions approaching those of perfect mixing were possible. Since these conditions gave the best stage efficiencies observed, it was decided to focus attention on them. The best flow rates for this purpose were 0.021 liter/sec. for the Isopar-H and 0.088 liter/sec. for water.

Residence time data were obtained as absorbance vs. time following the pulse dye injection and were converted to dimensionless normalized residence time probability using the relation

$$RTP = \frac{dF(t)}{d(t/\bar{t})} = \frac{\bar{t}\,\rho_{TW}Q_W}{M_{T0}} \tag{1}$$

where $F(t)$ is the residence time distribution function (*11* to *13*), $\bar{t}$ is the average residence time, ρ_{TW} the concentration of tracer in the water phase leaving the stage at a volumetric flow rate Q_W, and M_{T0} is the original amount of tracer injected into the continuous phase. For the case of interest here, a perfectly mixed stage, the residence time probability distribution is

$$RTP = \frac{dF(t)}{d(t/\bar{t})} = e^{-t/\bar{t}} \tag{2}$$

Representative experimental residence time probability distributions are compared with Equation (2) in Figures 6 and 7. Curves 1, 3 and 4, of Figures 6 and 7 are for pulse volumes of 50 cc. and curve 2 of Figure 6 for a pulse volume of 100 cc. In all cases identical masses of tracer were injected, and the curves show little variation in shape and average residence time, with the exception of curve 4 which represents a deviation from the desired mixing conditions as discussed below. Similar curves to those shown in Figures 6 and 7 were also obtained with a pulse volume of 5 cc., indicating that the injection volume had little effect on the residence time distribution or flow condition within the stage.

Although effluent dye concentration did not reach values predicted by the perfect mixing model until $t/\bar{t} \approx 0.2$, the observed distribution agreed more closely with this

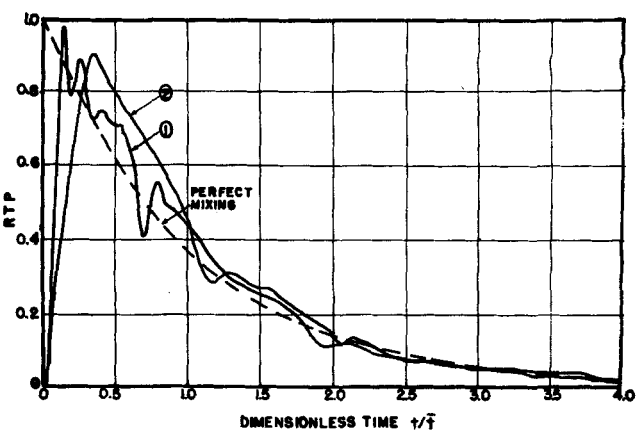

Fig. 6. Mixing characteristics of the continuous phase (curve 1, $\bar{t}$ = 84.79 sec.; curve 2, $\bar{t}$ = 81.59 sec.) for 0.021 liter/sec. Isopar-H and 0.088 liter/sec. water.

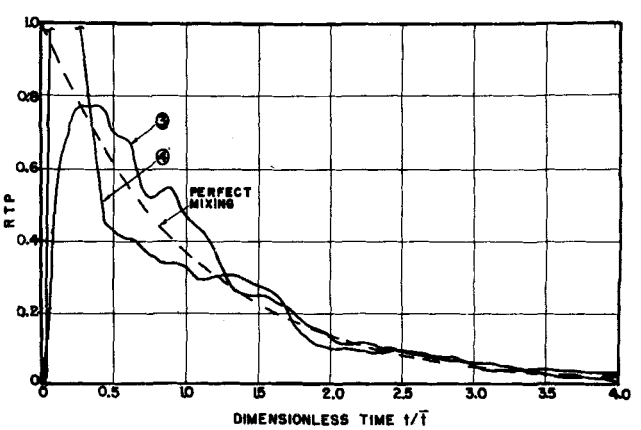

Fig. 7. Mixing characteristics of the continuous phase (curve 3, $\bar{t}$ = 81.05 sec.; curve 4, $\bar{t}$ = 67.18 sec.) for 0.021 liter/sec. Isopar-H and 0.088 liter/sec. water.

model for larger time. In addition, it was determined from visual observation that there was no bypassing of the stage and no area unaccessible to the dye. It was, therefore, assumed that the perfect mixing model would form an acceptable basis for estimating mass transfer behavior of the stage. However, in the fourth run pictured in Figure 7, behavior was significantly different. Here a substantial portion of the stream passed quickly out of the stage with little effective contact with the rising drops. This type of behavior is believed to be responsible for the occasionally observed unusually low extraction efficiency. A by-pass flow model was found to explain this behavior. Flow rates in all four runs were 0.021 liter/sec. for Isopar-H and 0.088 liter/sec. for water. Sensitivity of flow patterns to conditions of operation appears to be a major obstacle in the way of effective description and control of the column.

producibility of flow patterns was not really satisfactory. It seems, however, that these fluctuations may be closely connected to the inertia of the fluid leaving the downcomer. Residence time distributions of the drop phase were obtained from the measured velocities of the drops. The mean residence times for the individual drops were based on an effective stage height of 55 cm., calculated as the difference between the 24 in. (60 cm.) plate spacing and the thickness of the coalesced Isopar layer (5 cm.).

The measurements were made from drop data obtained from at least three independent stage efficiency experiments, using a flow rate of 0.021 liter/sec. for Isopar and 0.088 liter/sec. for water. The interfacial area and volumetric holdup in the stage varied from about 530 sq.cm. and 57 cc. for 450 drops to 670 sq.cm. and 72 cc. for 600 drops. However, the ratio of total interfacial area to total volumetric holdup remained essentially constant for the stage. Values of 9.14, 9.02, 9.20, and 9.46 (average =

TABLE 4. OBSERVED AND PREDICTED MASS TRANSFER FOR LIQUID EXTRACTION STAGE IN MODEL EXTRACTOR*

Solute distribution coefficient extraction factor	Average experimental NTU_D	Predicted NTU_D for average drop holdup of 550 surface-stretch	rigid sphere	Average experimental E_{MD}**	Average predicted E_{MD}** surface-stretch	rigid sphere
1. benzyl alcohol $m = 0.182$ $\xi = 0.0434$	0.3253	0.3439	0.0890	0.2777	0.2910	0.0852
2. dl-α-methylbenzyl alcohol $m = 0.590$ $\xi = 0.1408$	0.2157	0.2581	0.0682	0.1940	0.2275	0.0659
3. acetophenone $m = 10.268$ $\xi = 2.4503$	0.0426	0.0376	0.0107	0.0417	0.0369	0.0106

* All values based on average flow rates of 0.021 liter/sec. for Isopar-H and 0.088 liter/sec for distilled water.
** Calculated from average NTU_D.

Dispersed Phase

The Isopar-H drops moved upward through the continuous phase in a zig-zag fashion but with little backmixing, so that they could be considered to rise essentially in plug flow. The drops were observed to be oscillating between a near spherical shape and an oblate spheroidal configuration. Normally, the drops rise vertically to the top of the stage in a chimney as illustrated in Figure 8 for the perfectly mixed case. Occasionally, however, the drops tended to segregate toward the exit downcomer. As illustrated in Figure 8 for the case of bypassing. Drop patterns were not stable, and the causes of the pattern changes are unknown and unpredictable; hence, the re-

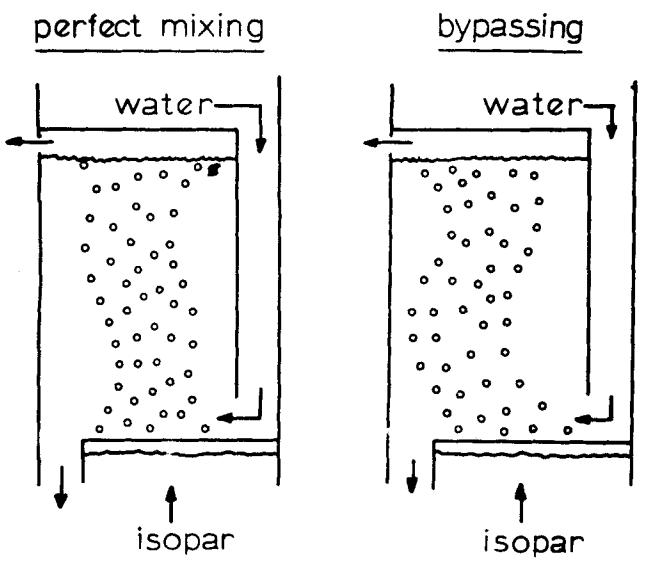

Fig. 8. Schematic diagram of dispersed phase flow in extraction stage.

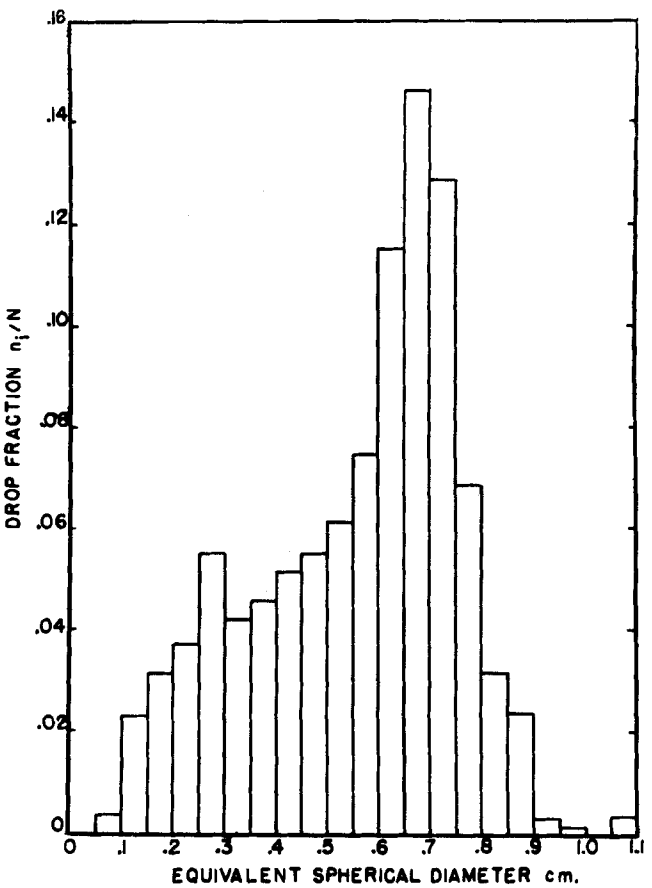

Fig. 9. Drop size distribution in model extractor for Isopar-H drops in water at 0.021 liter/sec. for Isopar-H and 0.088 liter/sec. for water. The total number of drop observations was 1,406.

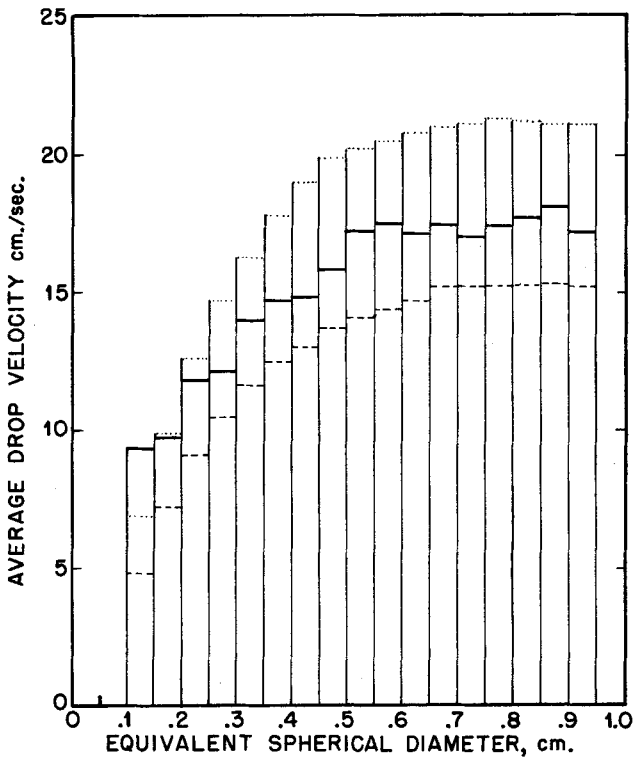

Fig. 10. Drop velocity distribution in model extractor for Isopar-*H*. Drops in water at 0.021/sec. for Isopar-*H* and 0.088/sec. for water. The total number of observations was 876. The dashed lines are terminal velocities calculated from the correlation of Hu and Kintner (*10*). The dotted lines are slip velocities calculated from the correlation of Liou (24).

9.20) for four determinations were obtained with a total of 1,406 drop observations. The observed drop size distribution is given in Table 3. This distribution, also shown in Figure 9, is the one used in subsequent mass transfer calculations. Individual drop velocities for 876 of the 1,406 observations were calculated and a number average velocity determined for each size class. This distribution of velocities is also given in Table 3 where it is compared with the corresponding terminal drop velocities, estimated from the well known correlation of Hu and Kintner (*10*). An additional comparison was made with the slip velocity of a single drop rising against a counter currently flowing field (*24*). These measured and calculated velocity distributions are compared in Figure 10. They are important in design work and their differences should be noted. The work presented by Lapidus and Elgin (25 to 29) represents a more extensive documentation method for drop velocity and drop holdup.

MASS TRANSFER BEHAVIOR

Once flow models have been established for the two fluid phases, it is possible to make a meaningful analysis of mass transfer effectiveness. One can calculate the Murphree stage efficiency, or an equivalent measure of stage performance, and relate this performance to the behavior of the individual drops. One can then compare observed mass transfer effectiveness, with predictions based on available models for droplet mass transfer.

Experimental Stage Efficiency

The Murphree stage efficiency E_{MD} based on the drop phase was found from the fractional solute extraction f by:

$$E_{MD} = \frac{f}{\xi(1-f)} \tag{3}$$

$$\xi = \frac{mQ_I}{Q_W} \tag{4}$$

Here f is simply the ratio of the solute extracted by the Isopar phase to the total amount injected, m is the distribution coefficient, ξ is the extraction factor, and Q_I and Q_W are the average volumetric flow rates of Isopar-H and water, respectively.

Equation (3) was derived for plug flow of the dispersed phase through a well-mixed continuous phase (*2*), the model chosen above. However, it can readily be shown (*2*) that calculated E_{MD}'s are not very sensitive to the flow model for the conditions of operation studied, unless there is substantial bypassing. The drops entered the stage with no solute.

Now, assuming that the drop phase is in plug flow in a well mixed continuous phase, the number of over-all mass transfer units can easily be determined from the Murphree stage efficiency [Equations (3) and (4)] by the well known relation:

$$NTU_D = [K_D(S/V)t] = -\ln(1 - E_{MD}) \tag{5}$$

The extractor performance was measured for the three solutes given in Table 2. The experimental data, which include mass transfer contributions from drop formation, rise, and coalescence, are given in Table 4 in terms of Murphree stage efficiency and numbers of transfer units. These values were calculated using Equations (3) to (5). They are compared here with predictions from the surface stretch and rigid sphere models.

Table 5. Predicted Mass Transfer Effectiveness During Drop Formation in Model Extractor

Solute	NTU_D	E_{MD}
1. benzyl alcohol	0.0297	0.0293
2. dl-α-methylbenzyl alcohol	0.0221	0.0219
3. acetophenone	0.0031	0.0031

Predicted Stage Efficiency

In this section the flow models just discussed are used in conjunction with available single-drop mass transfer models to estimate mass transfer effectiveness of the model extractor under the experimental conditions for which data were taken.

The Formation Period. Mass transfer during drop formation in the model extractor used here has been analyzed by Angelo, Lightfoot, and Howard (*3*). This analysis, based on the surface stretch model of mass transfer and experimental observation of drop growth, led to the expression

$$K_D = \sqrt{\frac{4\mathcal{D}_{AD}(1+\beta_S+\beta_S^2/3)}{\pi\, t_F}} \left[\frac{1}{1+m\sqrt{\mathcal{D}_{AD}/\mathcal{D}_{AC}}}\right] \tag{6}$$

Here K_D is the time average over-all mass transfer coefficient, based on drop-phase concentrations for the complete growth cycle of a representative drop. It is based on the remaining surface area just after break-off, S_0. For the operating conditions used in this study $\beta_S = 3.05$ and $t_F = 0.1147$ sec. Mass transfer effectiveness during drop formation was predicted by Equations (5) and (6) for the three solutes used in this study and are shown in

Table 5. These predictions are based on the assumption of uniform drop growth conditions, in accordance with the above values of β_S and t_f at each active orifice.

No corresponding calculations were made on the basis of fixed interface boundary-layer models. As it is clear (3) that surface growth must necessarily produce far higher mass transfer rates than predicted by such models.

The Rise Period. Estimates of mass transfer effectiveness during drop rise were made for both surface stretch and rigid sphere models of mass transfer, using observed drop trajectories. This was done by estimating the amount of solute picked up by drops in each size class and summing over all sizes. In making these calculations it was assumed that drop vibration frequency and amplitude are not affected by drop interaction, and the drops rise in plug flow through a well mixed continuous phase. It then follows that fractional solute extraction in the stage is expressed by

$$f = 1 - \left(\frac{\rho_{A2}}{\rho_{A1}}\right)_W = \frac{1}{1 + (Q_W/\Gamma)} \tag{7}$$

in which

$$\Gamma = \frac{m}{Z} \sum_{i=1}^{N} V_i n_i (v_{zi})_{\text{avg.}} (1 - e^{-NTU_{Di}}) \tag{8}$$

and

$$NTU_{Di} = \left[K_{Di} \frac{Z}{(v_{zi})_{\text{avg.}}} \cdot \frac{S_i}{V_i} \right] \tag{9}$$

The derivation of this equation is available elsewhere (2). Corresponding Murphree efficiencies and numbers of transfer units were calculated from Equations (3) to (5).

For the surface stretch model, mass transfer coefficients were calculated from the previously developed (3) relation

$$K_D = \sqrt{\frac{4\mathcal{D}_{AD}\omega(1 + \epsilon_0)}{\pi}} \left[\frac{1}{1 + m\sqrt{\frac{\mathcal{D}_{AD}}{\mathcal{D}_{AC}}}} \right] \tag{10}$$

which assumes a surface time relation for oscillating drops, the ones observed in the model extractor, of the form

$$\frac{S}{S_0} = 1 + \epsilon \sin^2(\pi\omega t) \tag{11}$$

where

$$\epsilon_0 = \epsilon + 3/8\ \epsilon^2 \tag{12}$$

In these calculations an average value of drop amplitude, $\epsilon = 0.2$ was used (based on Rose-Kintner (17) data) since, as can be seen from Equation (10), the oscillation amplitude is of minor importance compared to the vibration frequency. Vibration frequencies were estimated from the relation (19)

$$\omega = \frac{1}{2\pi} \sqrt{\frac{\sigma b}{D^3} \cdot \frac{192}{(3\rho_D + 2\rho_C)}} \tag{13}$$

and ranged from 30/sec. to 3.0/sec. for drops 0.15 to 0.95 cm. in diameter.

The Coalescence Period. No allowance was made for mass transfer during coalescence in the model extractor since the total interfacial area for coalescence (125 sq. cm.) is only about one-fifth of that of the rise period, and the rate of surface renewal is much less than that of the droplet phase, that is, the frequency of oscillation of the drops.

The predicted *NTU* values in Table 4 are, therefore, just the sum of the predictions based on the formation and rise periods alone. Extraction efficiencies in turn were calculated from the total transfer units by Equation (5).

The Effect of Surfactants: It is well known that the mass transfer behavior for systems containing surfactants often approximates that based on the rigid sphere mass transfer model. Therefore, rigid sphere mass transfer coefficients were used to predict what stage efficiency could be expected if the system was contaminated by surfactants.

The values for the formation number of transfer units calculated from the surface stretch model should also apply even in the presence of surfactants. Here it is assumed that short formation times (0.1147 sec.) and continual addition of surface elements from the bulk of the droplet phase retard the accumulation of foreign particles on the drop surface. Furthermore the mass transfer behavior during coalescence was again assumed negligible.

Rigid sphere mass transfer predictions for the rise period were made the same as before using Equations (7) through (9) to estimate the fractional extraction and Equations (3) through (5) for predicting stage efficiencies and number of transfer units, respectively. Over-all droplet phase mass transfer coefficients were estimated through the combination of an individual mean continuous phase mass transfer coefficient calculated from Froessling's (5) equation:

$$N_{ShC} = \frac{k_C D}{\mathcal{D}_{AC}} = 2 + 0.6\, N_{Re}^{1/2}\, N_{ScC}^{1/3} \tag{14}$$

and an individual mean drop phase coefficient calculated using Grober's (9) equation, as suggested by Skelland and Wellek (20):

$$k_D = -\frac{6}{D} \ln \frac{1}{\pi^2} \sum_{n=1}^{\infty} B_n e^{-(4\lambda_n^2 \mathcal{D}_{AD} t/D^2)} \tag{15}$$

The coefficients calculated from Equations (14) and (15) were combined into an over-all dispersed phase coefficient using the two resistance theory.

Comparisons between observed and predicted mass transfer behavior are shown in Table 4. The predictions of the surface stretch model are in reasonably good agreement with the experimental results and there is no observable effect of the distribution coefficient. Predictions of the number of transfer units based on the rigid sphere model, on the other hand, are only 1/3 to 1/4 of those observed, and again there is no observable effect of distribution coefficient.

The surface stretch and rigid sphere predictions for the rise period were made for an average drop holdup of 550. This was the average value counted from eight separate photographs. Each photograph was for a separate run. Figure 11 shows the relation between the observed drop holdup in the stage and the predicted number of transfer units for drop rise. It was used to prepare Table 6 in which drop holdup is calculated as required to predict maximum and minimum experimental numbers of transfer units. This range of required drop holdups compares reasonably well with observed variability (450 to 650), although observations were too few to permit statistical analysis.

It is of interest, however, that a few runs gave much lower mass transfer effectiveness than the average. Possible reasons for this are discussed in the next section.

Table 6. Drop Holdup Required for Observed Minimum and Maximum Number of Mass Transfer Units

Solute	Drop holdup required for observed $(NTU_D)_{\text{min.}}$	observed $(NTU_D)_{\text{max.}}$
1. benzyl alcohol	450	640
2. dl-α-methylbenzyl alcohol	440	500
3. acetophenone	620	640

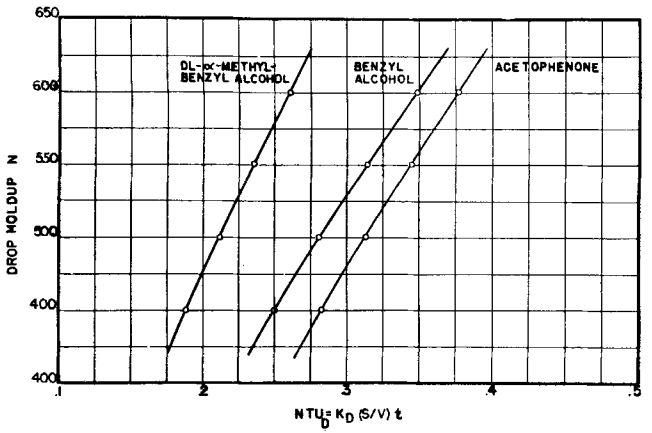

Fig. 11. Drop holdup vs. number of mass transfer units for 0.021 liter/sec. Isopar-*H* and 0.088 liter/sec. water. Calculations were based on the distributions of Figures 9 and 10. *NTU* values for acetophenone have been multiplied by ten.

BYPASS FLOW MODEL

To account for the unusually low observed stage efficiency occurring during some of the runs, a model featuring bypass flow was found successful. Here we imagine the incoming fluid as splitting into two parallel streams consisting of the fluid passing through the stage, and the fluid bypassing it. Levenspiel (*12*) gives a method of estimating the fraction of material bypassing the stage from a knowledge of the residence time probability distribution. If one plots the internal age distribution function

$$I = 1 - \int_0^{(t/\bar{t})} \frac{dF(t)}{d(t/\bar{t})}\, d(t/\bar{t}) \qquad (16)$$

as a function of $t/\bar{t}$, the resulting graph is indicative of the age of the elements within the stage. Such a plot is shown in Figure 12 and was prepared from the residence time probability distribution curve 4 on Figure 7.

As an example, we consider two of the *dl*-α-methylbenzyl alcohol runs for which low efficiencies were observed and which were not averaged with the values in Table 4. The average fractional extraction for the two runs was 0.0155 whereas that corresponding to the data in Table 4 was 0.0266. From Figure 12 we see that only about 53% of the incoming stream contacted the droplet phase so the estimated fraction extraction is about 0.014, very close to the observed average. For benzyl alcohol, the value of fractional extraction predicted by the bypass model is 0.0064 compared to the measured value of 0.0064. These calculations, therefore, appear to explain the low values of stage efficiency obtained and substantiate the use of residence time distributions for prediction of stage efficiency.

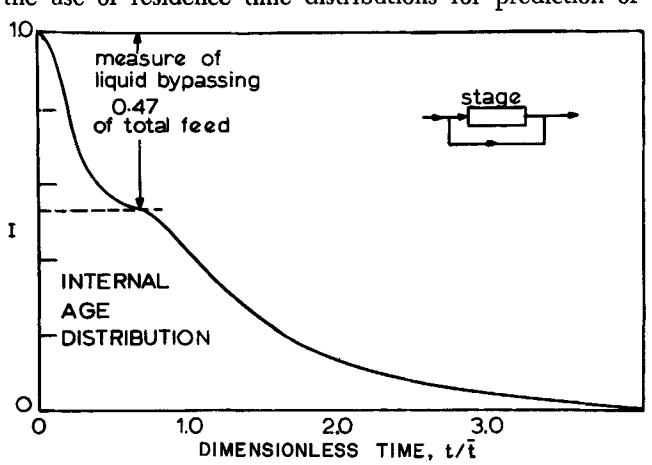

Fig. 12. Internal age distribution for bypass flow.

DISCUSSION

The most significant result of this research is the encouraging agreement between the observed mass transfer behavior and that predicted by the surface stretch mass transfer model and a reasonable flow model. Also of real importance is the demonstrated sensitivity of flow patterns to changes in operating conditions. The results strongly indicate the need for a much more thorough investigation of the fluid mechanic behavior of the column and suggest a radical change in geometry.

Mass Transfer

The agreement between observations and predictions based on surface stretch are a rather conclusive demonstration of system purity. It was shown that purity could be maintained by careful cleaning of equipment and solvents, and use of oxide free surfaces. No flow model consistent with residence time distributions and visual observations could give an observed mass transfer effectiveness equivalent to rigid sphere behavior.

The agreement between observations and predictions is a strong indication that the surface stretch model is a reasonable one but is not sufficient to distinguish between the Rose-Kintner analysis (*17*) and the surface stretch modification (*3*). A comparison of these two models is discussed elsewhere (*3*). It does, however, seem established that the droplet vibration frequency and amplitude are not greatly affected by droplet interaction, an important point. This is in line with single drop findings, but more convincing evidence for the surface stretch model is needed.

The change of the distribution coefficient did not greatly affect the degree of agreement between predictions and observations. Since the relative resistance of the two phases is proportional to the distribution coefficient, this is an indication of the validity of the Angelo and Lightfoot two film model. However, more data are needed for a conclusive check.

It also appears that the formation period is not important compared to the rise period in the stage for the conditions used. Here, too, however, further confirmation is desirable.

The flow model used was adequate as the results were sensitive to flow conditions only in the presence of bypassing. However, the two dimensional column used in this work may not give results that are directly translatable into a three dimensional environment, due to the wall effect and its effect on backmixing which was neglected.

Fluid Flow

Hydrodynamic drop interactions were quite pronounced within the stage. The drop holdup is not predictable from any known correlation, and as a result meaningful prediction of stage efficiency is not possible without measurement of the drop holdup. Channeling of drops was frequently very severe, and drop velocities were always in excess of individual drop terminal velocities.

Flow patterns in both phases were highly sensitive to flow conditions; the most serious effect of this is bypassing. The causes of pattern changes are not known and the reproducibility of flow patterns was not really satisfactory. It seems, however, that these fluctuations may be closely connected to the inertia of the fluid leaving the downcomer.

Drop formation at the orifice plate was unpredictable because many holes were not working and the pattern of working holes was not stable. This is probably because the pressure drop in the orifice is small compared to the local

pressure fluctuations below and above the orifice. Perhaps it is connected to the continuous phase patterns and certainly to drop patterns below the tray. This may be a major problem with this type of equipment.

In summary, it appears that the major uncertainty is in the flow patterns, and it hardly seems worthwhile refining the mass transfer calculations until flow conditions can be better controlled and understood. Fixing hydrodynamic conditions is a necessity in order to completely define the extraction process.

ACKNOWLEDGMENT

The authors wish to express their appreciation to Messrs. W. N. Hauser, Don E. Zentner, and Kerwin B. Spencer who were responsible for the construction and maintenance of the model extractor and its instrumentation. The valuable assistance of D. W. Howard with a number of experimental runs is also appreciated. In addition, we wish to thank the National Science Foundation, Wisconsin Alumni Research Foundation, The Sinclair Oil Company, and the Department of Chemical Engineering and the Engineering Experiment Station at Wisconsin for the financial support of this project. Finally, we wish to thank the Humble Oil and Refining Co. for supplying specially distilled Isopar-H in the large quantities needed.

NOTATION

A = absorbance or optical density, dimensionless
D = drop diameter or equivalent spherical diameter; D_i for a drop in size class i, L
$E_{MD} = \left(\frac{\rho_{A2}}{\rho_{A2}^*}\right)_D$ = Murphree stage efficiency for drop phase, dimensionless
$F(t)$ = residence-time distribution function, dimensionless
$m = \rho_{AI}^*/\rho_{AW}^*$ = distribution coefficient, dimensionless
M_{T0} = mass of tracer material injected into water phase at $t = 0$, M
Q_i = volumetric flow rate of phase i, L^3/t
t = time, t
Z = effective vertical rise height of drops, L

Greek Letters

β_S = surface growth rate constant for forming drop, dimensionless
ϵ = dimensionless amplitude for oscillating drops
ϵ_0 = dimensionless constant defined by Equation (12)
μ = viscosity, M/Lt
σ = interfacial tension, M/t^2
ρ_C, ρ_D = fluid density of continuous and dispersed phases, M/L^3
ρ_{Ai} = mass concentration of solute species A in phase i; $i = I, W, D$ or C
ξ = extraction factor defined by Equation (4), dimensionless
ω = droplet vibration frequency, t^{-1}

Dimensionless Groups

$N_{Re} = [D(v_z)_{\text{avg.}}\rho_C/\mu_C]$ = Reynolds number for drops
$N_{We} = [D(v_z)^2_{\text{avg.}}\rho_C/\sigma]$ = Weber number for drops
$N_{Sc_i} = [\mu_i/\rho_i \mathcal{D}_{Ai}]$ = Schmidt number; $i = D$ or C
$N_{Sh_i} = [k_i D/\mathcal{D}_{Ai}]$ = Nusselt number; $i = D$ or C
$NTU_D = [K_D(S/V)t]$ = number of over-all mass transfer units, for drop phase

Overlines and Superscripts

$-$ = time average value
$*$ = equilibrium value

Subscripts

A = solute species
C = continuous phase
D = drop phase
F = formation period
i = a given size class or fluid phase
I = Isopar-H
T = tracer
W = water phase
1 = entering stream
2 = leaving stream
0 = original or initial value, reference value
obs = observed value
calc = calculated value

LITERATURE CITED

1. Allerton, J., B. O. Strom, and R. E. Treybal, *Trans. Am. Inst. Chem. Engrs.*, **39**, 361 (1943).
2. Angelo, J. B., Ph.D. thesis, Univer. Wisconsin, Madison, Wisc. (1966).
3. Angelo, J. B., E. N. Lightfoot, and D. W. Howard, *AIChE J.*, **12**, 751 (1966).
4. Damon, K. G., J. B. Angelo, and R. W. Park, *Chem. Eng. Sci.*, **21**, 813 (1966).
5. Froessling, N., *Beitr. Geophysik*, **52**, 170 (1938).
6. Garner, F. H., S. R. M. Ellis, and D. W. Fosbury, *Trans. Inst. Chem. Engrs. (London)*, **31**, 348 (1953).
7. Garner, F. H., S. R. M. Ellis, and J. W. Hill, *AIChE J.*, **1**, 85 (1955).
8. Goldberger, W. M., and R. F. Beneati, *Ind. Eng. Chem.*, **51**, 645 (1959).
9. Grober, H., *Z. Ver. Deut. Ing.*, **69**, 705 (1925).
10. Hu, S., and R. C. Kintner, *AIChE J.*, **6**, 281 (1960).
11. Kramers, H., and K. R. Westerterp, "Elements of Chemical Reactor Design and Operation," Chap. 3, Academic Press, New York (1963).
12. Levenspiel, O., "Chemical Reaction Engineering," Chap. 9, Wiley, New York (1962).
13. Levenspiel, O., and K. B. Bischoff, "Advances in Chemical Engineering," Vol. 4, p. 95, Academic Press, New York (1963).
14. Mayfield, F. D., and W. L. Church, *Ind. Eng. Chem.*, **44**, 2253 (1952).
15. Murall, K., and M. R. J. Rao, *J. Chem. Eng. Data*, **7**, 468 (1962).
16. Olney, R. B., and R. S. Miller, "Modern Chemical Engineering," Vol. I, pp. 89-139, Reinhold, New York (1963).
17. Rose, P. M., and R. C. Kintner, *AIChE J.*, **12**, 530 (1966).
18. Row, S. B., J. H. Koffolt, and J. R. Withrow, *Trans. Am. Inst. Chem. Engrs.*, **37**, 559 (1941).
19. Schroeder, R. R. and R. C. Kintner, *AIChE J.*, **11**, 5 (1965).
20. Skelland, A. H. P., and R. M. Wellek, *ibid.*, **10**, 491 (1965).
21. Treybal, R. E., "Liquid Extraction," 2 ed., McGraw-Hill, New York (1963).
22. Treybal, R. E., *Ind. Eng. Chem.*, **54**, 55 (1962); **53**, 161 (1961); **52**, 262 (1960); **51**, No. 3, Part II, 378 (1959); **50**, No. 3, Part II, 463 (1958); **49**, No. 3, Part II, 514 (1957); **48**, No. 3, Part II, 510 (1956).
23. Treybal, R. E. and F. E. Dumoulin, *Ind. Eng. Chem.*, **34**, 709 (1942).
24. Liou, David, MS thesis, Illinois Inst. Tech., Chicago, Illinois (1965).
25. Weaver, R. E. C., Leon Ladipus, and J. C. Elgin, *AIChE J.*, **5**, 533 (1959).
26. Beyart, B. O., Leon Lapidus, and J. C. Elgin, *ibid.*, **7**, 46 (1961).
27. Quinn, J. A., Leon Lapidus, and J. C. Elgin, *ibid.*, **7**, 260 (1961).
28. Bridge, A. G., Leon Lapidus, and J. C. Elgin, *ibid.*, **10**, 819 (1964).
29. Dunn, I., Leon Lapidus, and J. C. Elgin, *ibid.*, **11**, 158 (1965).

Manuscript received September 7, 1966; revision received September 29, 1967; paper accepted October 2, 1967. Paper presented at AIChE Salt Lake City Meeting.